sites along run-of-river impoundments (n = 13), the mean sample scores for the first DCA axis did not differ from those of free-flowing sites (115.8 versus 102.7, $P = 0.095$), suggesting that floristic recovery may occur.

To conclude, the storage reservoirs developed a river-margin vegetation that is permanently different from that in free-flowing rivers. In run-of-river impoundments, some floristic variables deteriorated, whereas others recovered in the long term, supporting the contention that fragile and resilient qualities may be combined in a single community (*17*). Our results have implications for river management. First, impounding boreal rivers for hydroelectric purposes, thus changing naturally sloping rivers to stairs of dams and level water bodies and offsetting seasonal fluctuations in flow, will obstruct the maintenance of species diversity. Second, accurate assessments of community responses to hydrological disruption of rivers require multivariate approaches. Given that the majority of the world's rivers are regulated (*3*), the results may raise the requirements on future dam licensing and relicensing to modify dam operation in such ways that ecological effects might be alleviated (*18*).

REFERENCES AND NOTES

1. R. J. Naiman, H. Décamps, M. Pollock, *Ecol. Appl.* **3**, 209 (1993).
2. H. Décamps, *ibid.*, p. 441.
3. B. L. Turner II *et al.*, Eds., *The Earth as Transformed by Human Action* (Cambridge Univ. Press, New York, 1993); M. Dynesius and C. Nilsson, *Science* **266**, 753 (1994).
4. I. G. Attwell, *Biol. Conserv.* **2**, 189 (1970); W. C. Johnson, R. L. Burgess, W. R. Keammerer, *Ecol. Monogr.* **46**, 59 (1976); P. W. Reily and W. C. Johnson, *Can. J. Bot.* **60**, 2410 (1982); S. B. Rood and S. Heinze-Milne, *ibid.* **67**, 1744 (1989); K. M. Dunham, *Afr. J. Ecol.* **28**, 200 (1990).
5. C. Nilsson, A. Ekblad, M. Gardfjell, B. Carlberg, *J. Appl. Ecol.* **28**, 201 (1991).
6. D. M. Rosenberg, R. A. Bodaly, P. J. Usher, *Global Environ. Change* **5**, 127 (1995).
7. In the storage reservoirs, live storage capacities ranged between 8.6 and 5900 Mm^3, water-level fluctuations ranged between 1.3 and 34.5 m during the growing season, and corresponding shoreline widths were between 8.3 and 700 m. In the run-of-river impoundments, water-level fluctuations ranged between 0.3 and 2.5 m during the growing season, and bank widths between 0.3 m and 70 m. The Lule, Pite, Skellefte, Ume, Ångerman, Indal, Ljungan, and Ljusnan rivers were chosen for study. These rivers all rise in the mountain chain that forms the border between Norway and Sweden and empty into the Gulf of Bothnia. Regulated water bodies on the rivers were systematically chosen to control for variation in location, size, and age of regulation, and exact site locations within water bodies were randomly chosen along their northern side.
8. The definition of a species follows T. O. B. N. Krok and S. Almquist [*Svensk Flora: Fanerogamer och Ormbunksväxter* (Esselte, Uppsala, Sweden, ed. 26, 1984)]. Percentage cover was estimated for trees and shrubs (>0.25 m), and for dwarf shrubs (<0.25 m) and herbs. Bank height was measured as the vertical distance between the highest and lowest water levels during the growing season. Substrate types were classified according to particle size into peat, clay, silt, sand, gravel, pebbles, cobbles, boulders, and bedrock. Substrate fineness was calculated by weighing values of mean particle size by percentage composition of the river margin substrate, and substrate heterogeneity was calculated as the total number of substrate types at each site [C. Nilsson, G. Greisson, M. Johansson, U. Sperens, *Ecology* **70**, 77 (1989)].
9. Species richness was transformed with the formula: richness = number of species/$\log_{10}$ of area sampled [E. F. Connor and E. D. McCoy, *Am. Nat.* **113**, 791 (1979)].
10. Free-flowing sites were random, independent samples from the Torne, Kalix, Pite, and Vindel rivers [C. Nilsson *et al.*, in (*8*); (*5*); C. Nilsson *et al.*, unpublished data]. To control for regional variation among sites, we compared storage reservoirs with free-flowing sites along the upstream halves of the rivers and run-of-river impoundments with free-flowing sites along their downstream halves. Available evidence [J. Lundqvist, *Botaniska Data om Norra Sveriges Vattenområden* (National Natural History Museum, Stockholm, 1970); H. Sjörs, *Om Botaniska Skyddsvärden vid Älvarna* (Uppsala University, Uppsala, Sweden, 1973)] confirms that, before hydroelectric exploitation, riparian vegetation was similar between the regulated and free-flowing rivers, especially if sites in similar regions are compared. Sampling of free-flowing sites comprised the entire range (from 2.2 to 158 m) between the highest and lowest water levels during the growing season.
11. J. C. Trexler and J. Travis, *Ecology* **74**, 1629 (1993).
12. C. J. Gill, *Appl. Biol.* **2**, 129 (1977); T. T. Kozlowski, Ed., *Flooding and Plant Growth* (Academic Press, Orlando, FL, 1984); C. W. P. M. Blom and L. A. C. J. Voesenek, *Trends Ecol. Evol.* **11**, 290 (1996).
13. G. E. Petts, *Impounded Rivers: Perspectives for Ecological Management* (Wiley, Chichester, UK, 1984).
14. E. Hörnberg, *The Rivers Umeälven and Vindelälven. Part 2, Shore Development* (Umeå University, Umeå, Sweden, 1974); C. Nilsson, *Acta Phytogeogr. Suec.* **69**, 1 (1981).
15. J. S. Hanson, G. P. Malanson, M. P. Armstrong, *Ecol. Model.* **49**, 277 (1990).
16. The analyses were made with the program CANOCO [C. J. F. ter Braak, *Update Notes: CANOCO Version 3.10* (Agricultural Mathematics Group, Wageningen, Netherlands, 1990)], with default settings, and latitude and longitude as covariables to control for geographical variation in the flora.
17. G. Orians in *Unifying Concepts in Ecology*, W. H. Van Dobben and R. H. Lowe-McConnell, Eds. (Junk, The Hague, 1975); D. W. Schindler, *Can. J. Fish. Aquat. Sci.* **44**, 6 (1987).
18. B. Wuethrich, *Science* **272**, 344 (1996); M. Barinaga, *ibid.* **273**, 1648 (1996).

19. M. Dynesius, M. E. Johansson, B.-G. Jonsson, J. Moen, J. V. Ward, S. D. Wilson, and anonymous reviewers provided valuable comments on the manuscript. M. Danvind, M. Dynesius, M. E. Johansson, and M. Svedmark assisted in the field and M. Svedmark compiled background data. Supported in part by a grant from the Swedish Natural Science Research Council (to C.N.).

10 January 1997; accepted 27 February 1997

Defective Excitation-Contraction Coupling in Experimental Cardiac Hypertrophy and Heart Failure

A. M. Gómez, H. H. Valdivia, H. Cheng, Miriam R. Lederer, L. F. Santana, M. B. Cannell, S. A. McCune, R. A. Altschuld, W. J. Lederer*

Cardiac hypertrophy and heart failure caused by high blood pressure were studied in single myocytes taken from hypertensive rats (Dahl SS/Jr) and SH-HF rats in heart failure. Confocal microscopy and patch-clamp methods were used to examine excitation-contraction (EC) coupling, and the relation between the plasma membrane calcium current (I_{Ca}) and evoked calcium release from the sarcoplasmic reticulum (SR), which was visualized as "calcium sparks." The ability of I_{Ca} to trigger calcium release from the SR in both hypertrophied and failing hearts was reduced. Because I_{Ca} density and SR calcium-release channels were normal, the defect appears to reside in a change in the relation between SR calcium-release channels and sarcolemmal calcium channels. β-Adrenergic stimulation largely overcame the defect in hypertrophic but not failing heart cells. Thus, the same defect in EC coupling that develops during hypertrophy may contribute to heart failure when compensatory mechanisms fail.

Hypertensive disease can lead to cardiac hypertrophy and heart failure and is a major cause of death in developed countries. The heart failure that follows prolonged hypertension is characterized by decreased cardiac contractility and ejection fraction with sequelae that include pleural effusions, ascites, hepatic congestion, and atrial thrombi (*1*). Animal models of hypertension, cardiac hypertrophy, and heart failure show that pressure overload leads first to hypertrophy and then to a loss of contractile function (*1*, *2*). In healthy heart-muscle cells, electrical excitation leads to contraction because depolarization of the cardiac sarcolemmal membrane opens L-type Ca^{2+} channels (or dihydropyridine receptors, DHPRs), and the resulting local intracellular Ca^{2+} concentration ($[Ca^{2+}]_i$) increase activates SR Ca^{2+}-release channels (ryanodine receptors or RyRs). This Ca^{2+}-induced Ca^{2+}-release mechanism (*3*) depends on the high local $[Ca^{2+}]_i$ in the immediate vicinity of the DHPR to rapidly activate the

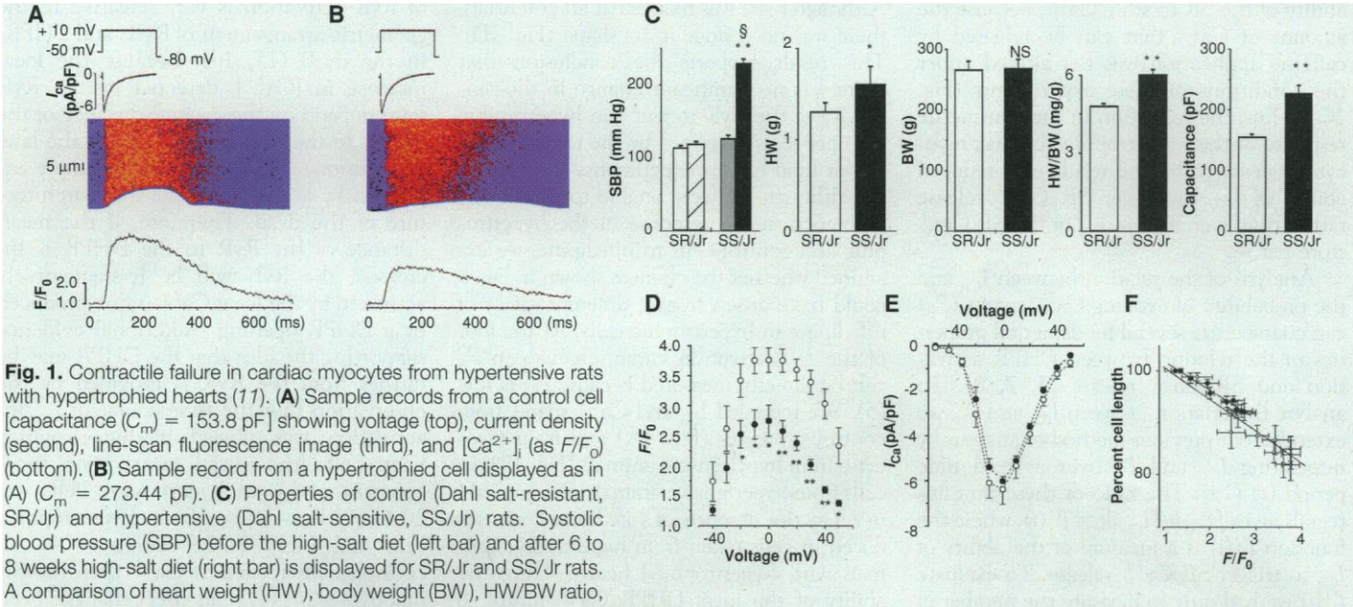

Fig. 1. Contractile failure in cardiac myocytes from hypertensive rats with hypertrophied hearts (*11*). (**A**) Sample records from a control cell [capacitance (C_m) = 153.8 pF] showing voltage (top), current density (second), line-scan fluorescence image (third), and $[Ca^{2+}]_i$ (as F/F_0) (bottom). (**B**) Sample record from a hypertrophied cell displayed as in (A) (C_m = 273.44 pF). (**C**) Properties of control (Dahl salt-resistant, SR/Jr) and hypertensive (Dahl salt-sensitive, SS/Jr) rats. Systolic blood pressure (SBP) before the high-salt diet (left bar) and after 6 to 8 weeks high-salt diet (right bar) is displayed for SR/Jr and SS/Jr rats. A comparison of heart weight (HW), body weight (BW), HW/BW ratio, and membrane capacitance is presented for SR/Jr and SS/Jr rats (after high-salt diets). Values are the mean ± SE with significance indicated as follows: $^*P < 0.05$ compared with SR/Jr rats; $^{**}P < 0.001$ compared with SR/Jr rats; $^{\S}P < 0.001$ compared with SS/Jr before high-salt diet. (**D**) Voltage dependence of $[Ca^{2+}]_i$ transients measured as peak F/F_0 for control cells (○) and hypertrophied cells (●). The fluorescent signal (F) was normalized to the signal before depolarization (F_0). (**E**) I_{Ca} current density–voltage relations for control cells (○) (n = 11) and hypertrophied cells (●) (n = 9). I_{Ca} was measured as the difference of the peak inward current and the steady-state current at the end of the 200-ms depolarization and plotted as current density (pA/pF). To control the SR Ca^{2+} load, we depolarized the cells for 50 ms at 0.1 Hz from −80 to 0 mV. (**F**) Relation between change in cell length and $[Ca^{2+}]_i$ (as peak F/F_0) in control (○) and hypertrophic (●) cells. Lines are linear regressions, $y = a + bx$, where values are for hypertrophic cells (a = 107.5 ± 0.8; b = −5.6 ± 0.3) and control cells (a = 107.2 ± 3.7; b = −6.5 ± 1.2).

local RyRs (*4*, *5*), and this process is facilitated by the close proximity of the DHPRs and RyRs in the dyad (*6*–*8*). Once activated by the Ca^{2+} influx through the DHPR, the RyR allows a larger amount of Ca^{2+} to move from the SR into the cytosol to activate contraction. The loss of contractility in heart failure can therefore be ascribed to changes in the Ca^{2+} transient or altered expression of myosin isoenzymes (*9*), or both.

A. M. Gómez, L. F. Santana, W. J. Lederer, Department of Physiology and the Medical Biotechnology Center, University of Maryland School of Medicine, 725 West Lombard Street, Baltimore, MD 21201, USA.
H. H. Valdivia, Department of Physiology, University of Wisconsin Medical School, Madisón, WI 53706, USA.
H. Cheng, Medical Biotechnology Center, University of Maryland School of Medicine, 725 West Lombard Street, Baltimore, MD 21201, and Section of Cardiovascular Research, National Institute of Aging, Baltimore, MD 21224, USA.
M. R. Lederer, Department of Physiology, University of Maryland School of Medicine, 725 West Lombard Street, Baltimore, MD 21201, USA.
M. B. Cannell, Department of Physiology and the Medical Biotechnology Center, University of Maryland School of Medicine, 725 West Lombard Street, Baltimore, MD 21201, USA, and Department of Pharmacology and Clinical Pharmacology, St. George's Hospital Medical School, London SW17 ORE, UK.
S. A. McCune, Department of Food Science and Technology, Ohio State University, Columbus, OH 43210, USA.
R. A. Altschuld, Department of Medical Biochemistry, Ohio State University, Columbus, OH 43210, USA.

*To whom correspondence should be addressed. E-mail: jlederer@umabnet.ab.umd.edu

The Ca^{2+} release from functional elements of the SR can be directly observed as Ca^{2+} sparks (*6*), the measurement of which gives the probability of release of Ca^{2+} from the SR (*7*, *8*). In principle, a reduction in the amplitude of the $[Ca^{2+}]_i$ transient in failing heart cells could arise from any of the following steps involved in EC coupling: (i) a reduction of I_{Ca} (which supplies the trigger for RyR activation); (ii) a reduction in the sensitivity of the RyR to the trigger Ca^{2+}; (iii) a change in the number of RyRs; (iv) a change in properties of the elementary SR Ca^{2+}-release events or Ca^{2+} sparks {because summation of these events leads to the cell-wide $[Ca^{2+}]_i$ transient (*6*)}; and (v) a reduction in the amount of releasable SR Ca^{2+} (*3*, *10*). Because hypertensive hypertrophy precedes overt heart failure, we first examined EC coupling changes in hypertrophy.

Single myocytes obtained from the hypertensive rat (Dahl SS/Jr) (*11*) with cardiac hypertrophy displayed smaller $[Ca^{2+}]_i$ transients and weaker contractions than myocytes from age-matched control animals (SR/Jr), whereas I_{Ca} density was similar (Fig. 1, A and B). There was a significant increase in systolic blood pressure (>100 mm Hg), an increase in heart weight, and cellular hypertrophy (shown by the expansion of cell surface area) in hypertensive animals (SS/Jr) as compared with control animals (SR/Jr) (Fig. 1C). In averaged data obtained in 11 control and 9 hypertrophic cells, the amplitude of the $[Ca^{2+}]_i$ transient (shown as F/F_0) was reduced (Fig. 1D), whereas the I_{Ca} current density (Fig. 1E) and the relation between peak $[Ca^{2+}]_i$ and cell contraction was unaltered (Fig. 1F).

The above results show that the reduced contractility of the cardiac cells from SS/Jr animals is largely explainable by the changes in the $[Ca^{2+}]_i$ transient, and the change in the $[Ca^{2+}]_i$ transient is not simply due to a change in I_{Ca}. A lack of effect of hypertrophy on I_{Ca} density has also been found in other animal models and in human cells, but these results may be model dependent (*2*, *12*). Therefore, the reduced contractility of the cardiac myocytes from hypertensive animals must result from a change in properties of the coupling of the DHPR to the RyR, a change in the properties of the Ca^{2+} sparks, or a change in the Ca^{2+} content of the SR. Images of Ca^{2+} sparks from control and hypertrophic myocytes were similar in appearance, having the same amplitude, the same kinetics of decay, and the same width. In both cases, the Ca^{2+} sparks were colocalized with transverse-tubules (Fig. 2B), the expected location of Ca^{2+} sparks (*6*, *7*). The reduction in the amplitude of the $[Ca^{2+}]_i$ transient in hypertensive animals is not simply explained by a change in the

ability of the SR to store Ca^{2+}, because the amount of Ca^{2+} that can be released by caffeine application was not altered under the conditions of these experiments (Fig. 2C). Thus, the reduction in the contractile response of the hypertrophied cardiac myocyte appears to be the result of a reduced ability of I_{Ca} to trigger SR Ca^{2+} release rather than a change in I_{Ca} or the SR Ca^{2+} store per se.

Analysis of the relation between I_{Ca} and the probability of evoking Ca^{2+} sparks (P_S) can characterize several fundamental properties of the relation between DHPR activation and SR Ca^{2+} release (*5*, *7*, *8*). To analyze the relation between I_{Ca} and P_S, we extended our previous method of analysis by integrating I_{Ca} and P_S over a fixed time period (t) (*13*). The ratio of these time integrals gives $\int P_S\,dt/\int I_{Ca}\,dt = f''(i)$, where the function $f''(i)$ is a measure of the ability of I_{Ca} to trigger SR Ca^{2+} release. To evaluate $f''(i)$ we had only to measure the number of Ca^{2+} sparks observed and integrate I_{Ca} during the voltage-clamp pulse. We could therefore quantitatively examine the effectiveness of the DHPR single-channel current to activate SR Ca^{2+} release (Fig. 3, A and B). Nifedipine was used to reduce the number of DHPRs opened by the voltage step to enable resolution of individual Ca^{2+} sparks (*7*, *8*). Integrating the current record reduced uncertainty due to noise in the raw records. The probability of evoking a Ca^{2+} spark for SR/Jr and SS/Jr myocytes was integrated over the 200-ms depolarization interval (Fig. 3C). In SS/Jr myocytes, there was a marked reduction in P_S at all potentials, although there was no significant change in either the density or voltage dependence of I_{Ca} (*14*). The voltage dependence of $f''(i)$ was reduced at all potentials and was statistically significant at 0 mV and at more negative potentials (Fig. 3D). These data show that, in myocytes from hypertensive animals, the local Ca^{2+} influx produced by DHPR openings is less able to activate SR Ca^{2+}-release units and (thereby) generate Ca^{2+} sparks. We examined the possibility that this result might arise from a change in the Ca^{2+} dependence of the open probability (P_O) of the RyR itself by incorporating purified SR vesicles into planar lipid bilayers. There was no detectable change in the single-channel current or the Ca^{2+} dependence of RyR open probability (Fig. 3F) in preparations from control and hypertrophic hearts. Furthermore, there was no change in the ryanodine binding to the purified SR vesicles (Fig. 3E), suggesting that the intrinsic properties of the RyRs were unaltered with regard to density or biochemical properties in the hypertensive animal. The shape of $f''(i)$ as a function of voltage can be used to examine the local Ca^{2+} dependence of RyR activation (*8*). Although $f''(i)$ was reduced at all potentials, there was no change in its shape (Fig. 3D). This result supports the conclusion that there was no significant change in the sensitivity of the RyR to Ca^{2+} in hypertrophic cells per se as suggested by the results of the planar lipid bilayer experiments (Fig. 3F).

Although we were unable to detect any difference in the response of the hypertrophic and control cells to nifedipine, we examined whether the changes shown in Fig. 3 could have arisen from a different effect of nifedipine in hypertrophic cells. At the foot of the I_{Ca} activation curve, changes in P_S can be directly measured because P_O is low (*5*). We recorded I_{Ca} and Ca^{2+} sparks from control myocytes (Fig. 4A) and from myocytes from hypertensive animals (Fig. 4B). In cells from hypertensive animals, $f''(i)$ at −44 mV (in the absence of nifedipine) was reduced in cells taken from hypertensive animals with hypertrophied hearts. Thus, the ability of the local DHPR Ca^{2+} influx to activate SR Ca^{2+} release is decreased in hypertrophic cells, without any detectable change in the properties of the RyRs.

If the properties of RyRs and DHPRs are unaltered in hypertensive animals, how can we explain the reduction in the ability of the DHPR to activate Ca^{2+} release? Mathematical analysis shows that the probability of RyR activation is very sensitive to the geometric arrangement of RyRs and DHPRs in the dyad (*15*, *16*). Because the local increase in $[Ca^{2+}]_i$ detected by the RyR must depend on the average distance of the DHPR to the RyR (as required by the laws of diffusion), our data could be simply explained by a change of the microarchitecture of the dyad. Therefore, if the mean distance of the RyR to the DHPR is increased, the RyR will be less effectively activated by the local Ca^{2+} influx produced by a DHPR opening. Additional evidence supporting the idea that the DHPR may be further from the RyR is provided by the observation that the time course of I_{Ca} inactivation was slowed in hypertrophied heart cells [the initial inactivation time-constant of I_{Ca} in hypertensive cells was 20.4 ± 2.5 ms (n = 18) in hypertrophied cells and 14.59 ± 0.9 ms (n = 44) in controls]. SR release of Ca^{2+} from the SR inactivates I_{Ca} (*17*), an effect that has been explained by the local increase in $[Ca^{2+}]_i$ (from RyR opening) promoting a rapid, Ca^{2+}-dependent inactivation of its neighboring DHPR and thereby accelerating the inactivation kinetics of I_{Ca}. Therefore, the slowing of I_{Ca} inactivation in hypertrophic cells would be consistent with the idea that the physical location of DHPRs with re-

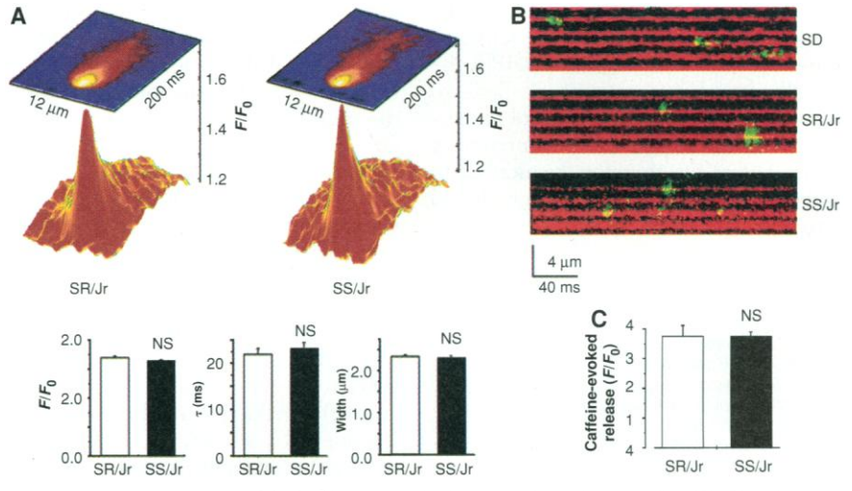

Fig. 2. Unitary properties of SR Ca^{2+} release in hypertrophied heart cells. (**A**) Signal-averaged Ca^{2+} sparks are shown as line-scan image (top) and a surface plot (bottom) from control cells and hypertrophic cells. No statistical differences are seen with respect to Ca^{2+}-spark magnitude (F/F_0), rate of decay (τ), and width (in micrometers at half-peak F/F_0) (control cells, n = 146; hypertrophic cells, n = 76). (**B**) The SR Ca^{2+} release takes place at the t-tubules (TT) in heart cells (*7*) from Sprague-Dawley control animals (SD, top), salt-resistant animals (SR/Jr, middle), and salt-sensitive hypertensive animals (SS/Jr, bottom). Sulpho–rhodamine B was used to identify the extracellular space in the TT (red), whereas Ca^{2+} sparks were imaged simultaneously (green) (*7*). Virtually all Ca^{2+} sparks appeared to originate at the TT/SR junction. (**C**) Ca^{2+} load was assessed in quiescent cells loaded with fluo-3 by the acetoxymethyl ester method (*4*, *5*) and by rapidly applying 10 mM caffeine extracellularly, which causes the Ca^{2+} in the SR to be released (*10*). To maintain conditions constant, we first regularly depolarized cells in normal Tyrode (2 mM $CaCl_2$) at 1 Hz for 2 min. Then, the caffeine-containing solution (with 0 mM Na^+ and 0 mM Ca^{2+} to block Na^+/Ca^{2+} exchange) was superfused over the cells. The peak F/F_0 upon the application of 10 mM caffeine was not statistically different ($P > 0.05$) for control cells (n = 9) and for hypertrophied cells (n = 26).

spect to their neighboring RyRs may be altered in hypertrophic cells (*18*). Furthermore, there are ultrastructural changes in the t-tubular system (and other structures) of hypertrophied hearts (*19*). Our results provide biophysical evidence that links such ultrastructural changes to a compromise in the ability of the local increase in $[Ca^{2+}]_i$ (due to DHPR openings) to activate SR Ca^{2+} release, which can be manifest as a loss of contractile function.

If EC coupling and contractility are compromised in hypertrophy, how is the heart able to eject blood at the (raised) arterial pressure? First, the increased cross section of the myocyte, due to the hypertrophy, will support the generation of more force. Second, there is an increase in sympathetic activity [see (*20*) and below]. The β-adrenergic agonist isoproterenol (1 μM) enhanced the reduced $f''(i)$ in myocytes from hypertensive animals to the level observed in control myocytes (Fig. 4, C and E). This enhancement also occurred in the absence of nifedipine at −44 mV (Fig. 4D). The increase of $f''(i)$ at all potentials by isoproterenol means that there is an enhanced efficacy of the Ca^{2+} influx (due to the opening of DHPRs) to activate SR Ca^{2+}-release units. Mechanistically, isoproterenol could enhance EC coupling by at least three means: (i) by increasing the mean open time of the DHPR (*21*), which may affect the local $[Ca^{2+}]$ sensed by RyRs (*15*); (ii) by increasing the sensitivity of the RyR to the local $[Ca^{2+}]$ as a result of A-kinase–dependent phosphorylation (*15*, *22*); and (iii) by increasing SR Ca^{2+} content, as a result of the increase of cyclic AMP produced by isoproterenol, via the phosphorylation of phospholambam and the consequent activation of the SR Ca^{2+} adenosine triphosphatase (*23*); and there is increasing evidence that SR Ca^{2+} levels also regulate RyR Ca^{2+} sensitivity (*4*, *10*, *24*). Because sympathetic drive is thought to be increased in pressure-overload hypertension (*1*, *20*, *25*), the ability of the hypertrophied cells to function effectively may be explained by a combination of the above mechanisms despite their defective EC coupling.

The changes in EC coupling associated with hypertension-induced hypertrophy that we have observed may not be related to the problem of heart failure. We therefore studied cells from 17- to 18-month-old SH-HF rats in overt heart failure (*26*) (Fig. 5). Each animal studied exhibited the typical signs of

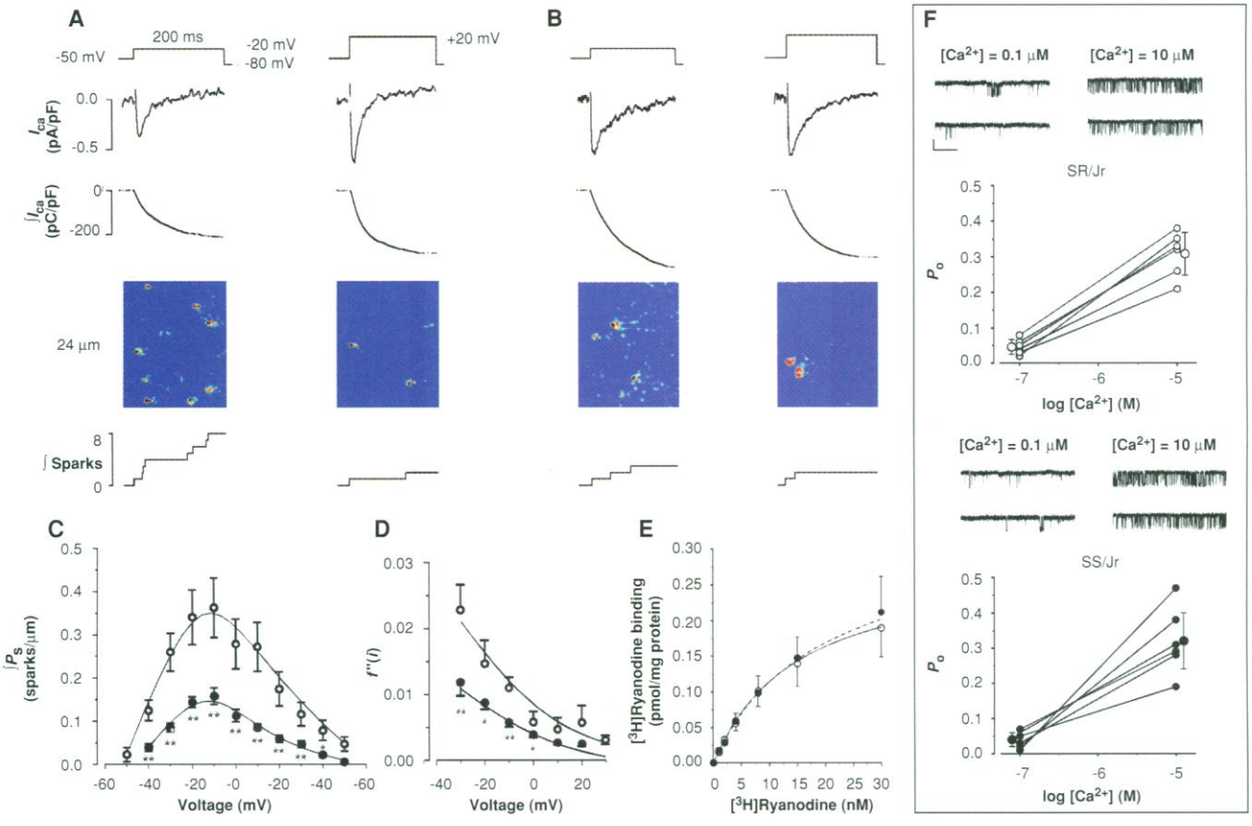

Fig. 3. The sarcolemmal Ca^{2+} current activates Ca^{2+} sparks less efficiently in hypertrophied cells than in control cells. (**A**) Control cells. Depolarizing steps to −20 and +20 mV (top) activate I_{Ca} (second panel), reflected as a running integral $\int I_{Ca}$ (third panel), triggering Ca^{2+} sparks (line-scan image shown in fourth panel) with a running integral of Ca^{2+}-spark occurrence (bottom). (**B**) Hypertrophic cells. Displayed as in (A). (**C**) Voltage dependence of $\int P_S$ over the 200-ms depolarization in control (○) and hypertrophic (●) cells (*29*). (**D**) Voltage dependence of $f''(i) = \int P_S / \int I_{Ca}$ = (sparks/μm)/(pC/pF) over 200 ms is shown for control cells (○) (n = 6) and for hypertrophic cells (●) (n = 7). $^*P < 0.05$; $^{**}P < 0.01$. The external solution contained 1 μM nifedipine to incompletely block I_{Ca} (*8*). The lines were visually fit and scaled to fit both data sets. (**E**) [³H]Ryanodine saturation binding curves for control (○) and failing (●) SR vesicles. K_d, the affinity constant of the [³H]ryanodine-RyR complex, was 15.2 ± 5.1 nM (control) and 18.3 ± 7.9 (hypertensive) (*30*); B_{max}, the maximal density of receptor sites, was 0.29 ± 0.09 (control) and 0.32 ± 0.08 (hypertensive) pmol/mg protein (n = 6 determinations from three rats each). Smooth lines are fits to data points with the formula $B = B_{max} \cdot [Ry]/([Ry] + K_d)$. (**F**) Single-channel records from RyRs incorporated into planar lipid bilayers (*22*, *30*). Holding potential, −30 mV in all traces. Openings are represented by downward deflections of the baseline current. Experiments were carried out at 100 nM $[Ca^{2+}]_i$, a level near resting $[Ca^{2+}]_i$, and at 10 μM $[Ca^{2+}]_i$, a level estimated to be close to that reached during local Ca^{2+}-induced Ca^{2+} release (*16*). Open probability (P_O) of the RyR from control (○) and from hypertrophied hearts (●) is shown to be indistinguishable. At pCa 7, P_O was 0.046 ± 0.021 (control) and 0.040 ± 0.019 (hypertensive). At pCa 5, P_O was 0.308 ± 0.06 (control) and 0.32 ± 0.08 (hypertensive). Vertical scale, 20 pA; horizontal scale, 300 ms.

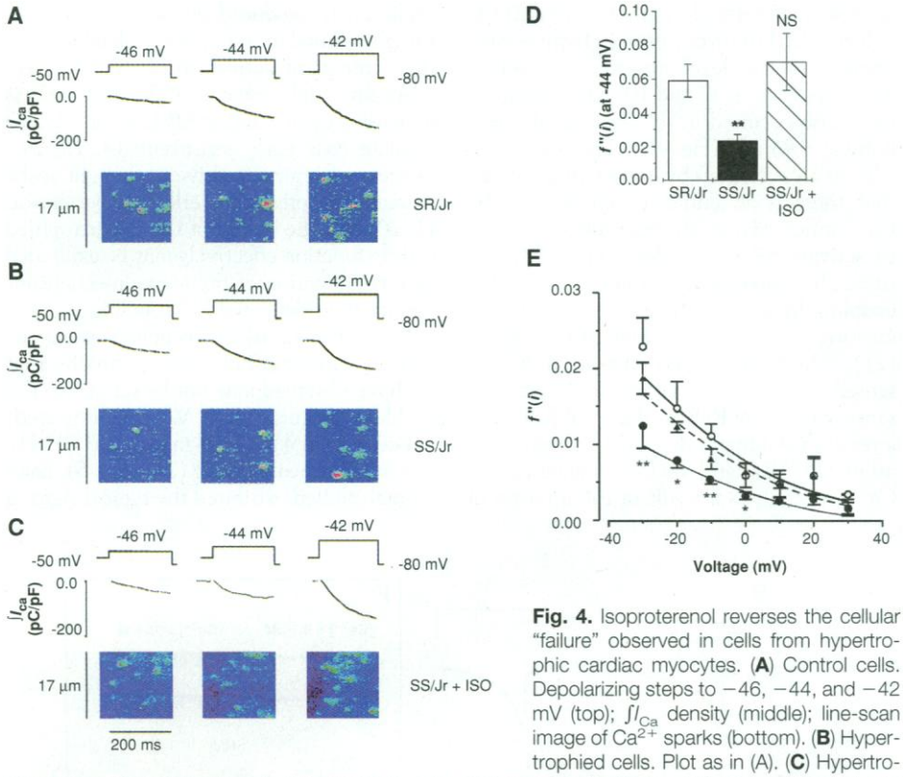

Fig. 4. Isoproterenol reverses the cellular "failure" observed in cells from hypertrophic cardiac myocytes. (**A**) Control cells. Depolarizing steps to −46, −44, and −42 mV (top); $\int I_{Ca}$ density (middle); line-scan image of Ca^{2+} sparks (bottom). (**B**) Hypertrophied cells. Plot as in (A). (**C**) Hypertrophied cells after exposure to isoproterenol (1 μM). Plot as in (A). (**D**) $f''(i) = \int P_S/\int I_{Ca}$ = (sparks/μm)/(pC/pF) over 200 ms plotted at −44 mV for cells taken from SR/Jr and SS/Jr animals and for SS/Jr animals after treatment with isoproterenol (1 μM). (**E**) $f''(i) = \int P_S/\int I_{Ca}$ plotted against voltage for control cells (○), for hypertrophic cells (●) (solid line), and for hypertrophic cells after treatment with isoproterenol (1 μM) (▲) (dashed line) (n = 7). The solution contained nifedipine (1 μM). There is no significant difference between control cells and SS/Jr cells after treatment with isoproterenol. Between SR/Jr and SS/Jr cells, significance is $^*P < 0.05$ and $^{**}P < 0.01$. Tetrodotoxin (10 μM) and no nifedipine was present in experiments shown in (A) through (D).

heart failure including cardiac hypertrophy, pulmonary congestion and pleural effusions, ascites, and hepatic congestion (*26*). Compared to cells from age-matched control animals, cells from animals in heart failure showed reduced cell shortening as a function of potential (Fig. 5C). Although the I_{Ca} density was unchanged, there was a reduction in the amplitude of the $[Ca^{2+}]_i$ transient at all potentials (Fig. 5, D and E). Furthermore, the ability of a given DHPR Ca^{2+} influx to activate SR Ca^{2+} release (as measured by Ca^{2+} sparks) was reduced in cells obtained from the hearts of animals in heart failure. Thus, myocytes from failing hearts appear to have a defect in EC coupling that is similar to that observed in cardiac myocytes taken from hypertensive animals.

Exposure of cardiac myocytes from failing hearts to isoproterenol produced almost no change in $f''(i)$ (Fig. 5F), in contrast to the effects of isoproterenol on myocytes from hypertrophic hearts that were not failing (Fig. 4E). This result suggests that the defect in EC coupling that develops in hypertrophy is not compensatable by β-adrenergic stimulation in failing hearts and may explain in part why these hearts fail. The marked increase in circulating catecholamines observed in heart failure is accompanied by a down-regulation of the β-adrenergic receptors (*27*). It is not clear, however, whether down-regulation of the cardiac β-adrenergic receptors is the cause or effect of the increased levels of catecholamines.

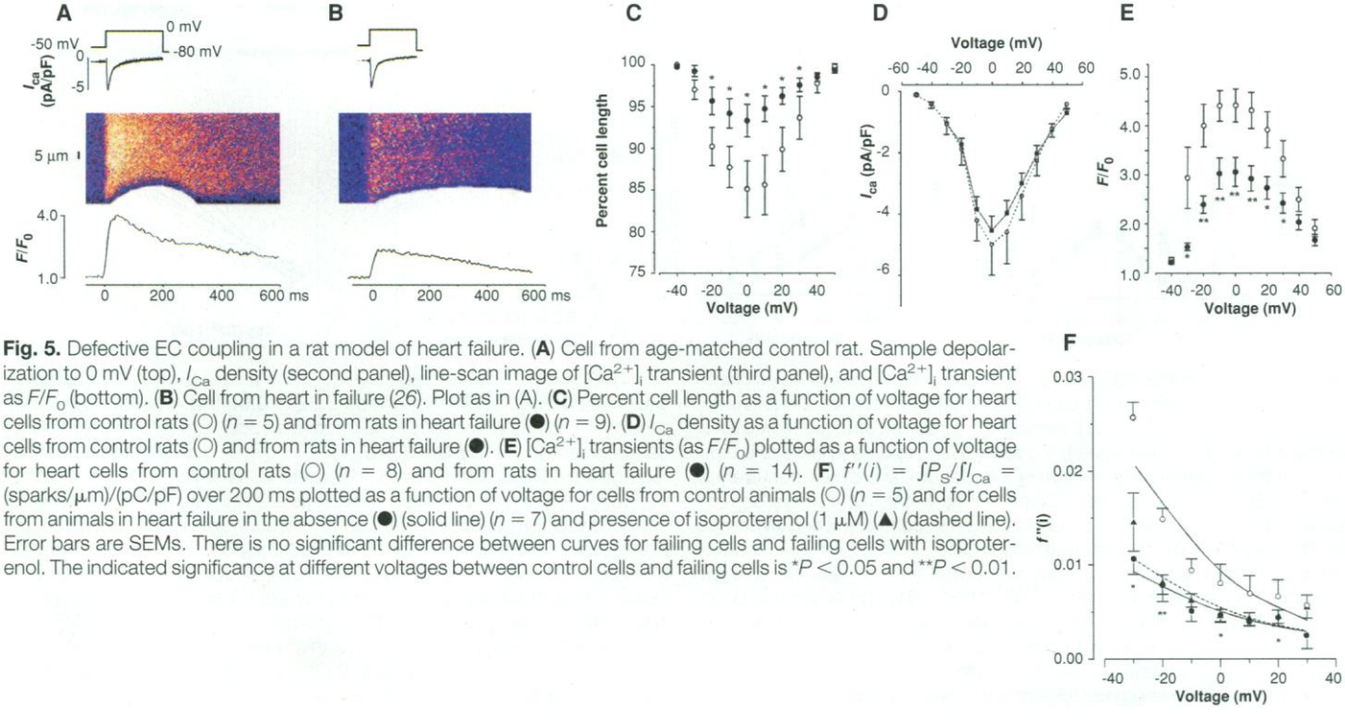

Fig. 5. Defective EC coupling in a rat model of heart failure. (**A**) Cell from age-matched control rat. Sample depolarization to 0 mV (top), I_{Ca} density (second panel), line-scan image of $[Ca^{2+}]_i$ transient (third panel), and $[Ca^{2+}]_i$ transient as F/F_0 (bottom). (**B**) Cell from heart in failure (*26*). Plot as in (A). (**C**) Percent cell length as a function of voltage for heart cells from control rats (○) (n = 5) and from rats in heart failure (●) (n = 9). (**D**) I_{Ca} density as a function of voltage for heart cells from control rats (○) and from rats in heart failure (●). (**E**) $[Ca^{2+}]_i$ transients (as F/F_0) plotted as a function of voltage for heart cells from control rats (○) (n = 8) and from rats in heart failure (●) (n = 14). (**F**) $f''(i) = \int P_S/\int I_{Ca}$ = (sparks/μm)/(pC/pF) over 200 ms plotted as a function of voltage for cells from control animals (○) (n = 5) and for cells from animals in heart failure in the absence (●) (solid line) (n = 7) and presence of isoproterenol (1 μM) (▲) (dashed line). Error bars are SEMs. There is no significant difference between curves for failing cells and failing cells with isoproterenol. The indicated significance at different voltages between control cells and failing cells is $^*P < 0.05$ and $^{**}P < 0.01$.

Our data suggest that hypertension-induced cardiac hypertrophy leads to a progressive decrease in the ability of the DHPR to activate SR Ca^{2+} release. The same defect is present in heart failure, but the failing cells respond poorly to β-adrenergic stimulation. Because of the apparent benefit of isoproterenol in hypertrophy, it may be possible to develop drug or molecular therapies that improve cardiac contractility in heart failure. An agent that produces an increase in RyR $[Ca^{2+}]_i$ sensitivity should partly restore lost contractility, although any such effort must be constrained by a need to avoid "Ca^{2+} overload" and the associated arrhythmias (*28*).

REFERENCES AND NOTES

1. E. Braunwald, in *Heart Disease: A Textbook of Cardiovascular Medicine*, E. Braunwald, Ed. (Saunders, Philadelphia, ed. 3, 1988), pp. 426–445, 471–484.
2. D. J. Beuckelmann and E. Erdmann, *Basic Res. Cardiol.* **87**, 235 (1992); D. J. Beuckelmann, M. Näbauer, E. Erdmann, *Circulation* **85**, 1046 (1992); M. Arai, H. Matsui, M. Periasamy, *Circulation Res.* **74**, 555 (1994); G. Hart, *Cardiovasc. Res.* **28**, 933 (1994).
3. A. Fabiato, *J. Gen. Physiol.* **85**, 291 (1985); *ibid.*, p. 189; *ibid.*, p. 247; M. B. Cannell, J. R. Berlin, W. J. Lederer, *Science* **238**, 1419 (1987); W. H. duBell and S. R. Houser, *Cell Calcium.* **8**, 259 (1987); *Am. J. Physiol.* **257**, H746 (1989); L. Barcenas-Ruiz and W. G. Wier, *Circulation Res.* **61**, 148 (1987); M. Näbauer, G. Callewaert, L. Cleemann, M. Morad, *Science* **244**, 800 (1989); E. Niggli and W. J. Lederer, *ibid.* **250**, 565 (1990); D. M. Bers, *Excitation-Contraction Coupling and Cardiac Contractile Force* (Kluwer, Dordrecht, 1991).
4. H. Cheng, W. J. Lederer, M. B. Cannell, *Science* **262**, 740 (1993).
5. M. B. Cannell, H. Cheng, W. J. Lederer, *ibid.* **268**, 1045 (1995).
6. ———, *Biophys. J.* **67**, 1942 (1994).
7. ———, *J. Physiol. (London)* **477**, 25P (1994); H. Cheng, M. B. Cannell, W. J. Lederer, *Circulation Res.* **76**, 236 (1995); P. S. Shacklock, W. G. Wier, C. W. Balke, *J. Physiol. (London)* **487**, 601 (1995); J. R. López-López, P. S. Shacklock, C. W. Balke, W. G. Wier, *Science* **268**, 1042 (1995); H. Cheng, M. R. Lederer, W. J. Lederer, M. B. Cannell, *Am. J. Physiol.* **270**, C148 (1996); H. Cheng *et al.*, *Cell Calcium* **20**, 129 (1996).
8. L. F. Santana, H. Cheng, A. M. Gómez, M. B. Cannell, W. J. Lederer, *Circ. Res.* **78**, 166 (1996).
9. A. M. Lompré *et al.*, *Nature* **282**, 105 (1979); I. Dubus, J.-L. Samuel, B. Swynghedauw, *Eur. Heart J.* **14** (suppl.), 76 (1993).
10. R. A. Bassani and D. M. Bers, *Biophys. J.* **68**, 2015 (1995); C. I. Spencer and J. R. Berlin, *J. Physiol. (London)* **488**, 267 (1995); J. W. Bassani, W. Yuan, D. M. Bers, *Am. J. Physiol.* **268**, C1313 (1995); N. Negretti, A. Varro, D. A. Eisner, *J. Physiol. (London)* **486**, 581 (1995).
11. To produce hypertension and hypertrophy, we used a genetic strain of rats that become hypertensive when fed a high-salt diet (Dahl rats, strain SS/Jr). Control rats were a matched strain that remain normotensive when fed the same high-salt diet (Dahl rats, strain SR/Jr) [L. K. Dahl, M. Heine, L. Tassinari, *Nature* **194**, 480 (1962); J. P. Rapp and H. Dene, *Hypertension* **7**, 340 (1985); J. P. Rapp, *ibid.* **4**, 753 (1982); M. Inoko, Y. Kihara, I. Morii, H. Fujiwara, S. Sasayama, *Am. J. Physiol.* **267**, H2471 (1994)]. Heart cells from adult Sprague-Dawley rats produced results similar to those of the control Dahl rats (SR/Jr). The cells from hypertensive Dahl rats (SS/Jr) used in these experiments were hypertrophied as revealed by capacitance measurements as shown in Fig. 1C and supported by direct observation. Systolic blood pressure was measured in every animal, before the high-salt diet and the day of experiments, by the tail-cuff method in conscious animals, prewarmed in thermostatic cages at 37°C. The salt-sensitive SS/Jr rats become hypertensive after increasing dietary salt from 1 to 8%. This diet was maintained for 6 to 8 weeks. The salt-resistant SR/Jr strain did not become hypertensive after the same dietary protocol and served as the genetic and physiologic control. As noted above, all of the findings in the control SR/Jr rat heart cells were indistinguishable from results seen in heart cells obtained from Sprague-Dawley rats (Charles River Labs) weighing 250 to 300 g and fed a diet of normal rat Chow without water restriction. Single rat cardiac myocytes were dissociated by enzymatic treatment as described (*8*). Whole-cell currents were monitored with an Axopatch 200A patch-clamp amplifier. Series resistance was electronically compensated. Data were recorded and analyzed with pCLAMP 6.01. During experiments, cells were superfused with an external solution containing 135 mM NaCl, 1 mM $MgCl_2$, 20 mM CsCl, 10 mM glucose, 10 mM Hepes, 3 mM 4-aminopyridine, 1 mM $CaCl_2$ (pH 7.4). In some experiments tetrodotoxin (10 μM) was added. Patch pipettes were filled with 130 mM CsCl, 0.1 mM fluo-3, 10 mM Hepes, 0.33 mM $MgCl_2$, 20 mM tetraethylammonium chloride, 4 mM MgATP (pH 7.2). All images were acquired with a Bio-Rad MRC 600 confocal microscope fitted with an Ar ion laser and processed with Bio-Rad SOM, COMOS, and IDL (Research Imaging Systems, Boulder, CO) software. Data are presented as the mean ± SEM. Two-sample comparison was made by paired or independent t test, as appropriate. A level of $P < 0.05$ was assumed as statistically significant.
12. No change in I_{Ca} density was found in some models of hypertrophy, whereas some showed increases and others showed decreases. In hypertrophied cat ventricular myocytes [R. B. Kleiman and S. R. Houser, *Am. J. Physiol.* **255**, H1434 (1988)] or in pressure-overloaded guinea pigs or rats [F. Scamps, E. Mayoux, D. Charlemagne, G. Vassort, *Circ. Res.* **67**, 199 (1990); I. Primot, E. Mayoux, P. Oliviero, D. Charlemagne, *Cardiovasc. Res.* **25**, 875 (1991); A. M. Gómez *et al.*, *Am. J. Physiol.*, in press], I_{Ca} density was reported unchanged and was thought to be the general result in pressure-overloaded and aging myocardium [B. Chevalier *et al.*, *Basic Res. Cardiol.* **87** (suppl. 1), 187 (1992)]. Nevertheless, in other animal models changes in I_{Ca} have been identified. For example, in a model of infarction with hypertrophy [P. E. Santos, L. C. Barcellos, J. G. Mill, M. O. Masuda, *J. Cardiovasc. Electrophysiol.* **6**, 1004 (1995)] and in aortic banding model in guinea pig [Z. Ming, C. Nordin, F. Siri, R. S. Aronson, *J. Mol. Cell. Cardiol.* **26**, 1133 (1994)], I_{Ca} density was decreased. In the one-clip two kidney model, I_{Ca} was increased in heart failure [Q. Li and E. C. Keung, *Am. J. Physiol.* **266**, H1738 (1994)]. In the Dahl rat model presented here, I_{Ca} density was unchanged.
13. P_S should be the product of the probability that a DHPR is open (P_O) and the probability that the flux of Ca^{2+} through an open DHPR will activate SR Ca^{2+} release (P_i), or $P_S = P_O \cdot P_i$ (*5–8*). Because P_i should be a function [$f(i)$] of the local $[Ca^{2+}]$ change produced by the DHPR single-channel current (i) as well as the mean open time (τ) of the DHPR [$g(\tau)$], then $P_S = f(i) \cdot g(\tau) \cdot P_O$. Dividing both sides of this equation by the amplitude of the whole-cell Ca^{2+} current ($i \cdot n \cdot P_O$), $P_S/I_{Ca} = f(i) \cdot g(\tau) \cdot P_O/(i \cdot n \cdot P_O) = f'(i)\, g(\tau)$, where n is the number of Ca^{2+} channels in the cell. We measure P_S as a probability density function. However, P_S is an instantaneous probability that cannot be strictly determined by counting Ca^{2+} sparks over any time period, because I_{Ca} and hence P_S are time dependent. This problem can be circumvented by integrating P_S and I_{Ca} over the same fixed time period (T) to give $\int_T P_S\, dt / \int_T I_{Ca}\, dt = f'(i)$. $\int_T g(\tau)\, dt$ is a constant, so this term has been included in $f'(i)$ for the purpose of this analysis. Although changes in $g(\tau)$ can explain the reduction in P_S produced by inorganic DHPR antagonists (*6*), our current records do not indicate that large changes in the voltage dependence of $g(\tau)$ occur in these experiments.
14. A. M. Gómez *et al.*, data not shown.
15. C. Soeller and M. B. Cannell (personal communication) and numerical analysis of cardiac EC coupling [C. Soeller and M. B. Cannell, *Biophys. J.* **70**, A246 (1996)] suggest that the optimization of location of the DHPR with respect to the RyR to obtain the maximum SR Ca^{2+} release for the minimum DHPR Ca^{2+} influx ("tuning") is nearly maximal in normal heart cells. If this modeling "estimate" is correct, one may anticipate that the $f'(i)$ function may not be improved by increasing the RyR sensitivity to Ca^{2+} (for example, by exposure to isoproterenol and phosphorylation by A-kinase). However, small changes in the microarchitecture of the dyad may "de-tune" the system, which may then permit isoproterenol to improve $f'(i)$. Thus, in cardiac hypertrophy, an increase in the mean open time of the DHPR (τ) or an increase in the RyR sensitivity to local $[Ca^{2+}]$ induced by isoproterenol, or both, may increase $f'(i)$ by increasing $g(\tau)$or $f(i)$, or both (*13*), and thereby increase P_S.
16. M. D. Stern, *Biophys. J.* **63**, 497 (1992). See also (*6*).
17. J. S. K. Sham, L. Cleeman, M. Morad, *Proc. Natl. Acad. Sci. U.S.A.* **92**, 121 (1995); S. Adachi Akahane, L. Cleemann, M. Morad, *J. Gen. Physiol.* **108**, 1 (1996); C. J. Grantham and M. B. Cannell, *Circ. Res.* **79**, 194 (1996).
18. When Ba^{2+} is used as the charge carrier for I_{Ca}, no change in current inactivation between control and hypertrophic cells is observed (*14*). Because Ba^{2+} neither activates SR Ca^{2+} release nor inactivates DHPRs, this result suggests that the cause of the change in the time course of I_{Ca} inactivation is not due to a change in I_{Ca} gating per se.
19. E. Page and L. P. McCallister, *Am. J. Cardiol.* **31**, 172 (1973); K. Kawamura, C. Kashii, K. Imamura, *Jpn. Circ. J.* **40**, 1119 (1976); J. Schaper *et al.*, *Circulation* **83**, 504 (1991); F. Ferrante, E. Bronzetti, E. Ciriaco, L. Felici, F. Amenta, *J. Hypertens.* **10**, 507 (1992); see also (*1*). Although the reported changes do not provide the resolution needed to address the specific questions raised in our experiments, they are consistent with our findings.
20. E. Braunwald and J. Ross Jr., in *Handbook of Physiology: Section 2: The Cardiovascular System*, R. M. Berne, N. Sperelakis, S. R. Geiger, Eds. (American Physiological Society, Bethesda, MD, 1979), pp. 533–580. See also (*1*).
21. B. P. Bean, M. D. Nowycky, R. W. Tsien, *Nature* **307**, 371 (1984); T. F. McDonald, S. Pelzer, W. Trautwein, D. J. Pelzer, *Physiol. Rev.* **74**, 365 (1994).
22. H. H. Valdivia, J. H. Kaplan, G. C. R. Ellis-Davies, W. J. Lederer, *Science* **267**, 1997 (1995).
23. J. P. Lindemann, L. R. Jones, D. R. Hathaway, B. G. Henry, A. Watanabe, *J. Biol. Chem.* **258**, 464 (1983); A. D. Wegener, H. K. B. Simmerman, J. P. Lindemann, L. R. Jones, *ibid.* **264**, 11468 (1989); P. James, M. Inui, M. Tada, M. Chiesi, E. Carafoli, *Nature* **342**, 90 (1989).
24. N. Ikemoto, M. Ronjat, L. G. Mészáros, M. Koshita, *Biochemistry* **28**, 6764 (1989).
25. M. Esler, in *Hypertension: Pathophysiology, Diagnosis and Management*, J. H. Laragh and B. M. Brenner, Eds. (Raven, New York, ed. 2, 1995), pp. 755–773; N. Kaplan, in *Clinical Hypertension* (Williams and Wilkins, Baltimore, MD, 1990), pp. 95–100.
26. Spontaneously hypertensive SH-HF/Mcc-facp (SH-HF) rats have been selectively bred for congestive heart failure, and those carrying the *facp* (corpulent) gene, which encodes a defective leptin receptor [S. C. Chua Jr. *et al.*, *Science* **271**, 994 (1996)] have an earlier onset of the disease [S. A. McCune, P. B. Baker, H. F. Stills, *ILAR News* **32**, 23 (1990)]. Hearts from failing SH-HF rats exhibit mechanical alterations and the more negative force-frequency relation thought to reflect SR dysfunction in the failing rat myocardium [P. Narayan *et al.*, *J. Mol. Cell. Cardiol.* **27**, 523 (1995)], but SERCA2 protein is not decreased (R. M. Phillips, unpublished observations). Myocytes were isolated from four phenotypically lean 17- to 18-month-old male SH-HF rats heterozygous for the *facp* gene. Two animals were from the McCune colony at Ohio State University and two were from Genetic Models (Indianapolis, IN). M-Mode echocardiography [G. J. Haas, S. A. McCune, D. M. Brown, R. J. Cody, *Am.*

Heart J. **130**, 806 (1995)] under anesthesia (50 mg of ketamine per kilogram of body weight and 10 mg/kg xylazine) indicated that shortening fractions for the SH-HF rats (37 ± 3%) were significantly ($P < 0.01$) reduced relative to those of three 17- to 18-month-old Sprague-Dawley controls (57 ± 4%). Peak systolic blood pressure for the SH-HF rats was 164 ± 11 mm Hg versus 108 ± 10 mm Hg for the controls ($P < 0.02$). All of the failing rats had ascites, hydrothorax, and hepatic and pulmonary congestion; three also had large, well-resolved atrial thrombi. None of the controls exhibited these generally accepted signs of congestive heart failure.

27. M. R. Bristow *et al.*, *Circulation* **82**, 112 (1990); J.-M. Moalic, D. Charlemagne, P. Mansier, B. Chevalier, B. Swynghedauw, *ibid.* **87** (suppl. 4), IV21 (1993). See also (*1*, *25*).
28. F. T. Thandroyen *et al.*, *Circ. Res.* **69**, 810 (1991); C. T. January and H. A. Fozzard, *Pharmacol. Rev.* **40**, 219 (1988); C. Antzelevitch and S. Sicouri, *J. Am. Coll. Cardiol.* **23**, 1 (1994).
29. In our study we report $[Ca^{2+}]_i$ transient data as both F/F_0 and as Ca^{2+}-spark occurrence. To count Ca^{2+} sparks activated by I_{Ca}, the line-scan images were contrast-enhanced and displayed on a video monitor and visually counted. We also applied a spark-counting software algorithm (H. Cheng, unpublished data) to verify the result. The algorithm includes dividing the image by the fluorescence signal before depolarization, then low-pass filtering with a 1.5-μm, 15-ms spatiotemporal window. Spark events were objectively identified as discrete, isolated regions where fluorescence intensity exceeds the baseline mean intensity by $3\sigma^2$, where σ^2 is the variance of the baseline fluorescence. The results of both computer and visual spark-counting methods were in close agreement, with differences of less than 10%.
30. SR-enriched vesicles were isolated by differential centrifugation from whole hearts from control and hypertensive rats as described [C. A. Tate *et al.*, *J. Biol. Chem.* **260**, 9618 (1985)]. The fusion of microsomes into planar lipid bilayers revealed functional RyRs with properties similar to those of native RyRs; the analysis of single-channel kinetics was done as described [A. J. Lokuta, T. B. Rogers, W. J. Lederer, H. H. Valdivia, *J. Physiol. (London)* **487**, 609 (1995)]. Bilayers were composed of 50% phosphatidylethanolamine and 50% phosphatidylcholine (25 mg/ml in *n*-decane). The cis solution consisted of 300 mM $CsCH_3SO_3$, 10 mM Mops (pH 7.2), and EGTA:Ca^{2+} admixtures necessary to set free $[Ca^{2+}]$ to 100 nM and 10 μM. The trans solution was 50 nM $CsCH_3SO_3$ before SR fusion and 300 mM after fusion. Binding of [^{3}H]ryanodine to SR microsomes was performed for 90 min at 36°C in medium containing 0.2 M KCl, 10 mM NaCl, 1 mM AMP-PCP (a nonhydrolyzable analog of adenosine triphosphate), 1.6 mM $MgCl_2$ (0.6 mM free Mg^{2+}), 10 mM Na-Hepes (pH 7.2), and 20 μM $CaCl_2$ (10 μM free Ca^{2+}). The reaction was terminated by rapid filtration of samples. Nonspecific binding was determined in the presence of 10 μM ryanodine and has been substracted. Smooth lines are fits to data points with the formula $B = B_{max} \cdot [Ry]/([Ry] + K_d)$, where B is the specific binding and K_d is the dissociation constant. Protein concentration was determined by the Bradford method.
31. Supported by the Spanish Ministry of Education and Science (A.M.G.), Maryland Heart Association (H.C.), British Heart Foundation and Wellcome Trust (M.B.C.), NIH grants (L.F.S., H.H.V., S.A.M., R.A.A., and W.J.L.), and a Minority Scientist Development Award from the American Heart Association (H.H.V.). We thank C. Soeller for discussion of computer-modeling results; C. F. Neubauer, P. Sander, S. Park, J. Brenner, R. Ringel, J. Hensley, and K. O'Neill for technical support and for rat echocardiography; Hewlett-Packard for echo equipment; S. M. Wang for help in obtaining and maintaining Dahl rats; and J. Hamlyn, B. H. Scribner, D. Siscovick, and M. P. Blaustein for discussions on hypertension and heart failure.

5 November 1996; accepted 4 March 1997

Cell Cycle–Dependent Establishment of a Late Replication Program

M. K. Raghuraman,* Bonita J. Brewer, Walton L. Fangman

DNA replication origins in chromosomes of eukaryotes are activated according to a temporal program. In the yeast *Saccharomyces cerevisiae*, activation of origins in early S phase appears to be a default state. However, *cis*-acting elements such as telomeres can delay origin activation until late S phase. Site-specific recombination was used to separate origin from telomere in vivo, thereby demonstrating that the signal for late activation is established between mitosis and START in the subsequent G_1 phase. Once set, the signal can persist through the next S phase in the absence of the telomere. Establishment of the temporal program and of initiation competence of origins may be coincident events.

Eukaryotic chromosomes are organized into blocks of DNA sequence that replicate early in S phase interspersed with blocks that replicate late. Each temporal block is presumably replicated by the coordinate activation of clusters of replication origins (*1*). The functional significance of this temporal regulation remains open to speculation. A demonstrated correlation between actively transcribed genes and early replication in higher eukaryotes has led to the suggestion that early replication may be a prerequisite for the activation of gene transcription (*2*). Straying from the normal temporal program of replication may have deleterious consequences for development—for example, the fragile X syndrome is associated with delayed replication of the *FMR1* locus (*3*).

Saccharomyces cerevisiae chromosomes also contain early- and late-replicating domains, and yeast replication origins that are activated late in S phase have been identified recently (*4*–*6*). Although there has been much progress in understanding the molecular steps leading to the activation of replication origins (*7*), the molecular basis for the temporal program is less clear. The picture that is emerging is that yeast replication origins are activated early in S phase by default. Late activation, in those instances in which it has been found, is not an intrinsic property of the origins involved, but is imposed by *cis*-acting elements that are separable from the origin (*6*, *8*, *9*).

One example of a chromosomal element that affects origin activation time is the telomere—proximity to a telomere can cause late activation of origins (*8*, *10*). How the telomere effects a delayed schedule of origin activation is unknown, but the parallel phenomenon of telomeric position effect on transcription (*11*) suggests the involvement of a special chromatin structure propagated from the telomere. A notable feature of transcriptional silencing is its heritability: Silenced chromatin can be maintained and clonally inherited through several cell division cycles and, at least in the silent mating–type cassettes, maintenance of the repressed state can be independent of its initial establishment (*12*).

We now asked, first, if maintenance of the signal for late origin activation is also separable from its establishment by the telomere, and second, when in the cell cycle the telomeric late replication program is established. To address these questions, we used inducible, site-specific recombination to remove a subtelomeric late origin from its chromosomal location in vivo (Fig. 1). The excised circle, lacking determinants of late origin activation, is expected to replicate early in S phase unless the late replication signal originally established by the telomere persists after excision. Excising the origin at different times in the cell cycle would reveal if the telomeric late replication program is stably maintained for more than one round of the cell cycle or if it is reestablished in every cell cycle. For example, the origin can be removed at START, when the cell commits entry into another round of the cell cycle, and the cells then allowed to proceed through S phase. If the previously late origin now becomes active early in S phase, then the telomere must be needed after START and possibly through S phase to maintain the late replication program. If the origin remains late, then the program must be established before START and maintained through S phase in the absence of the telomere.

The origin excision cassette was constructed (*13*) in a strain that contains three copies of the "R" recombinase from *Zygosaccharomyces rouxii* under control of the GAL1 promoter (*14*) integrated in tandem at the *LEU2* locus on chromosome III. Tar-

Department of Genetics, University of Washington, Box 35-7360, Seattle, WA 98195–7360, USA.

*To whom correspondence should be addressed. E-mail: raghu@u.washington.edu